NANO LETTERS

Letter

pubs.acs.org/NanoLett

Controlled Interaction of Surface Quantum-Well Electronic States

Knud Seufert,[†] Willi Auwärter,*[,†,‡] F. J. García de Abajo,[§,∥] David Ecija,[†] Saranyan Vijayaraghavan,[†] Sushobhan Joshi,[†] and Johannes V. Barth[†]

[†]Physik Department E20 and [‡]Institute for Advanced Study, Technische Universität München, D-85748 Garching, Germany

[§]ICFO - Institut de Ciencies Fotoniques, Mediterranean Technology Park, 08860 Castelldefels, Barcelona, Spain

[∥]ICREA - Institució Catalana de Recerca i Estudis Avançats, Barcelona, Spain

ABSTRACT: We report on the construction of well-defined surface quantum well arrangements by combining self-assembly protocols and molecular manipulation procedures. After the controlled removal of individual porphyrin molecules from dense-packed arrays on Ag(111), the surface state electrons are confined at the bare silver patches. These act as quantum wells that show well-defined unoccupied bound surface states. Scanning tunneling spectroscopy and complementary boundary element method calculations are performed to characterize the interaction between the bound states of adjacent quantum wells and reveal a hybridization of wave functions resulting in bonding and antibonding states. The interwell coupling can be tuned by the deliberate choice of the molecules acting as potential barriers. The fabrication method is shown to be ideally suited to engineer specific configurations as one-dimensional chains or two-dimensional artificial molecules.

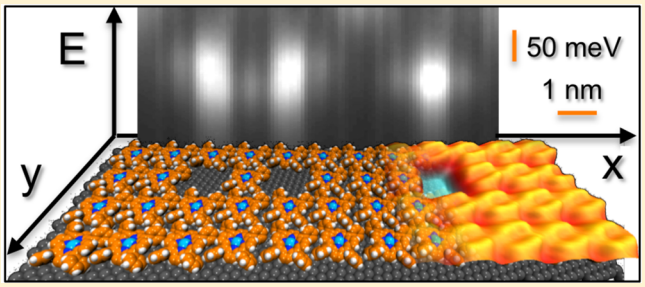

KEYWORDS: *Surface state, quantum dot, electron confinement, porphyrin, scanning tunneling microscopy (STM), scanning tunneling spectroscopy (STS)*

Many properties of matter emerge from the coupling of elementary quantum systems: Molecules, built from individual atoms, are bound via hybridized wave functions, whereas in crystalline solids consisting of periodic atomic arrays the overlap between neighboring sites determines the band structure and thus the electronic, optical, or magnetic behavior. Accordingly, the construction and exploration of artificial coupled quantum systems is of great interest, both from a fundamental scientific perspective and in view of potential applications in fields as materials engineering, molecular electronics, and quantum computing.[1−3] While progress in semiconductor technology allows designing quantum wells and dots with dimensions down to several nanometers in solid materials,[4−6] scanning tunneling microscopy (STM) permits the formation and characterization of coupled atomic quantum dots on hydrogen terminated silicon crystals.[7] More generally, STM on conducting surfaces opens up the fascinating possibility of building up structures consisting of just a few individual atoms or molecules and directly visualizing electron scattering and confinement. This grants access into the quantum nature of these systems[8,9] and enables the control of their electronic surface structures.[10,11]

On substrates supporting electronic Shockley surface states, mainly three approaches are established to build nanoscale assemblies affecting the pertaining quasi two-dimensional electron gas: (I) atomic manipulation to construct specific geometries,[8−12] (II) molecular self-assembly to form periodic networks[13−16] and (III) the use of adatom islands, vacancies or vicinal surfaces exhibiting regular arrays of steps.[17−21] Obviously, the latter approach is rather limited concerning the choice of geometry and symmetry. Methods (I) and (II) are somewhat complementary, as the serial atomic manipulation technique allows for the construction of specific configurations of limited extension,[22,23] while the self-assembly approach yields extended periodic structures.[13−15,24−27] In this Letter, we demonstrate a combined approach relying on both well-established molecular self-assembly protocols and STM manipulation, which guarantees fast preparation of tunable quantum well systems with the desired geometry. This method provides a rich playground to study electron confinement and to exquisitely steer the interaction of quantum wells, thus opening a new avenue to engineer the electron wave functions of complex systems.

Our STM experiments were performed in a custom-designed ultrahigh vacuum system providing a base pressure below 2×10^{-10} mbar. A monocrystalline Ag(111) substrate was cleaned by repeated Ar^+ sputtering cycles, followed by annealing at 730 K. Subsequently, a submonolayer coverage of porphyrins was deposited by organic molecular beam epitaxy from thoroughly degassed quartz crucibles. Both free-base (2H-TPP) and metalated (Co-TPP) tetraphenylporphyrins were sublimated to form extended highly regular arrays on Ag(111). Within the

Received: September 16, 2013
Revised: November 3, 2013
Published: November 18, 2013

   dx.doi.org/10.1021/nl403459m | *Nano Lett.* 2013, 13, 6130−6135

experimental precision, these arrays exhibit an identical square unit cell for both species with an intermolecular distance of 1.4 nm.[28,29] STM images were acquired using a low-temperature CreaTec-STM with the sample held at 6 K using electrochemically etched W tips. The lock-in modulation for STS measurements was typically 6 mV rms, which did not limit the resolution of the spectral features. The quantum wells were constructed by removing individual porphyrin modules via a STM manipulation technique: The tip was placed above the molecule to be removed and lowered toward the surface till a contact was achieved. Subsequently, the tip was retracted, pulling the molecule away from the surface (see Figure 1a), and laterally moved to a bare Ag(111) patch, where the molecule was dropped. Before repeating this process, the area of interest was scanned again, to guarantee that the desired molecule was targeted in the next iteration step. Typical parameters for this procedure are as follows: The tip is positioned applying regular imaging conditions, that is, a tunneling current of 0.3 nA and a sample bias voltage U_b of −0.666 V. For approach and retraction, U_b is set to 75 mV. The vertical tip displacement to contact the TPP varied with tip geometry and termination, a characteristic value is 5 Å resulting in a maximal current I of few hundred nanoamperes.

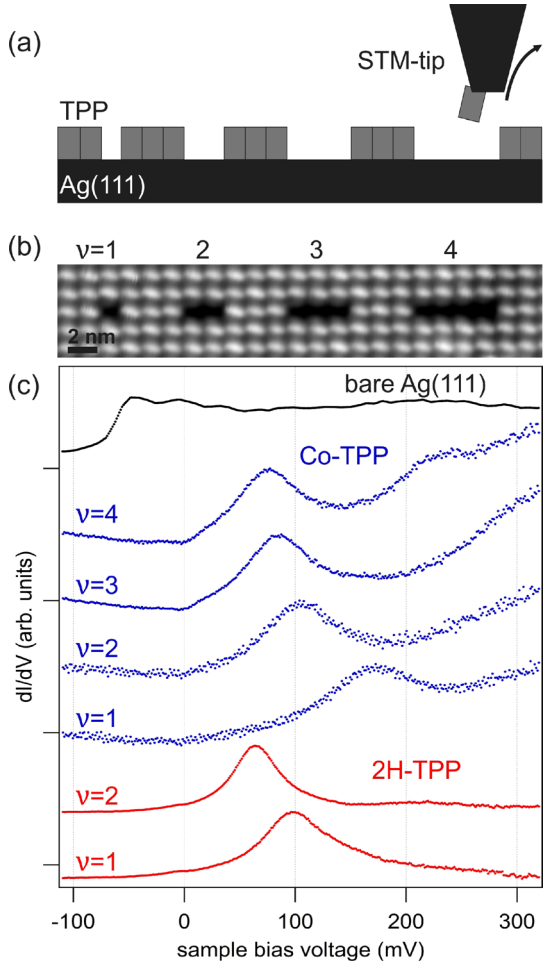

Figure 1. (a) Scheme outlining the construction of quantum wells in porphyrin (TPP) arrays on Ag(111) by means of STM manipulation. (b) STM image of four quantum wells in a Co-TPP matrix, exposing bare Ag trenches after the removal of ν = 1−4 molecules (U_b = −666 mV). (c) Scanning tunneling spectra representing the electronic structure in the center of trenches of different lengths (see labels) constructed on either Co-TPP (blue curves) or 2H-TPP (red curves) arrays (Tip positioned at U_b = −666 mV, I = 0.4 nA). A reference spectrum acquired on bare Ag(111) is shown for comparison (black curve). The onset of the surface-state band at about −65 mV is visible.

Our simulation of the STS data relies on calculations of the local density of states (LDOS) of electrons evolving in a two-dimensional (2D) potential landscape within the independent electron model. The potential is taken to be zero at the metal regions (supporting the surface-state of the clean metal surface) and V at the molecules region. A reasonable agreement with experiment is found by setting $V = (0.3-0.1i)$ eV for the free-base TPPs, where the imaginary part accounts for inelastic losses due to electron collisions with the molecules. The metal regions are described as squares for $\nu = 1$ quantum dots (QDs) and rectangles for $\nu > 1$, where ν is the number of missing molecules. We approximate the sidelength of a single QD to 1.4 nm, the spacing of TPP in the molecular arrays. The LDOS is then calculated by using the boundary element method (BEM) in which the electron wave function is constructed from a discrete dense set of boundary sources distributed along the boundaries. In particular, the LDOS is obtained from the imaginary part of the reflected wave function at the position of an "electron" point source, as explained in detail in the Supporting Information of ref 16.

Figure 1b shows a STM image of a porphyrin array after the construction of four quantum wells with well-defined shapes. Each quantum well consists of a bare Ag(111) patch following removal of ν Co-TPP molecules (ν = 1,..,4) (see Figure 1a). The porphyrin modules serve as potential walls reflecting and confining the surface-state electrons in the well, as inferred from scanning tunneling spectroscopy data presented in Figure 1c. Each spectrum, taken at the center of a well of different size, differs drastically from the reference spectrum acquired on the free Ag(111) surface, and displays well-defined peaks, typical for a confined electronic system.[8,13,30,31] It should be noted that the Ag(111) surface state is not detected by STS underneath the extended porphyrin arrays[29] and is possibly quenched. As expected from a simple particle-in-a-box picture, a decrease in length of the well (from ν = 4 down to 1, or equivalently, from a length of 5.6 nm down to 1.4 nm) results in an upshift of the first resonance (see Figure 1c). A detailed description and modeling of electron confinement in these rectangular wells will be presented elsewhere. Nonetheless, one important fact should be noticed: Comparison of two wells of identical size (e.g., ν = 1 or 2), but different environment (i.e., either Co-TPP or 2H-TPP walls), reveals that the first resonance is observed at lower energy for the free-base molecule. As the geometric footprint of both Co-TPP and 2H-TPP is essentially identical, this indicates that the latter confines the electrons less efficiently and thus represents lower-potential walls. The molecular backbone plays a relevant role in the scattering of surface-state electrons[32] but as both species exhibit a rather similar saddle-shape deformation of the macrocycle, we attribute the difference to the influence of the metal-center on the binding of the molecule to the substrate.[29,33]

Now we address the electronic interaction between quantum wells, focusing on the coupling of monovacancy species (ν = 1), which exhibit a nearly square geometric footprint. Figure 2a shows a STM topograph of two individual wells separated by a single 2H-TPP unit. Naturally, this dimeric configuration corresponds to the smallest possible geometric barrier thickness. The isolated well (monomer) located in the right part of

dx.doi.org/10.1021/nl403459m | Nano Lett. 2013, 13, 6130−6135

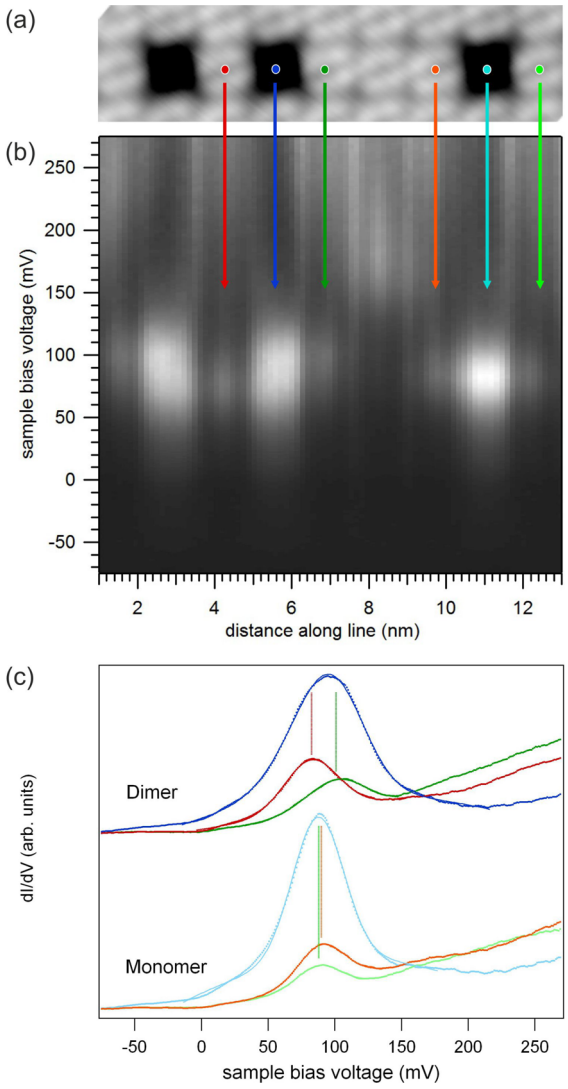

Figure 2. (a) STM image of a $\nu = 1$ dimer (left) and an individual reference well (right) in a 2H-TPP array ($U_b = 1$ V). The colored circles highlight the positions of the spectra reproduced in (c). (b) Spatially resolved STS space-energy map representing 101 single spectra taken along the axis connecting the three trenches in (a). (c) Comparison of characteristic spectra at selected positions near the individual (lower three spectra) and the coupled (upper three spectra) wells (offset for clarity; tip positioned at $U_b = -0.25$ V, $I = 0.5$ nA). The latter clearly support spectral components reflecting bonding and antibonding states. The solid curves represent Gaussian fits and the dashed lines mark the fitted peak positions after background subtraction.

Figure 2a serves as a reference. In order to explore the electronic properties of this structure, we recorded a series of tunneling spectra in the voltage range from −80 to 270 mV at 101 positions along the axis connecting the wells (Figure 2b). The central spectrum on the reference trench displays a peak centered at 88 mV with a full width at half-maximum (FWHM) of 45 mV (see Figure 2 light blue). In contrast, the feature dominating the spectra taken at the centers of the two neighboring wells is considerably broader (FWHM: 65 mV) and observed at a slightly higher energy (95 mV) (Figure 2 dark blue). This is a first hint that the close proximity of the two neighboring wells modifies their electronic structure and, therefore, they interact. More insight can be gained upon closer inspection of Figure 2b,c. Spectra taken at positions continuously entering the molecular walls enclosing the reference well show a decrease in peak intensity, corresponding to a reduction of electron density in the wall, equivalent to a decay of the probability density of the wave function in the barrier, while the peak position remains nearly constant. On the other hand, spectra recorded in the central barrier separating the two neighboring trenches and in the terminal walls on the outer side of the dimer exhibit a markedly different signature. Again, the peak intensity decreases when entering the walls, but the peak positions in both the central barrier (83 mV, red) and in the outer barrier (100 mV, green) are clearly shifted and distinct from the spectra in the vacancies. The two peaks shift in opposite directions and their width is reduced with respect to the spectrum at the center of one of the neighboring cavities (cf. dark blue and dark red/green curves, Figure 2c). This suggests that the broad spectral feature in the latter originates from a convolution of two peaks. Indeed, it can be nicely fitted by the superposition of two Gaussian curves centered at the energies of the low- and the high-energy components, respectively (see Figure 2c, dark blue solid curve). We find an intuitive explanation for this behavior in a simplified one-dimensional model. If two initially isolated quantum wells are brought in close contact, the primary isolated wave functions hybridize to form bonding (Ψ_n) and antibonding (Ψ_n^*) states. The bonding state, showing up at lower energy, has larger probability density inside the central barrier, while the higher-energy, antibonding state exhibits a node in the central barrier, accompanied by an increase in probability density in the outer walls. This is exactly what is observed in the experiment (Figure 2) and corroborated by boundary element method calculations presented in the following.

Figure 3 shows the calculated LDOS for two coupled quantum wells as a linescan (Figure 3a), a space-energy map (Figure 3b), and 2D energy maps (Figure 3c,d) in which a

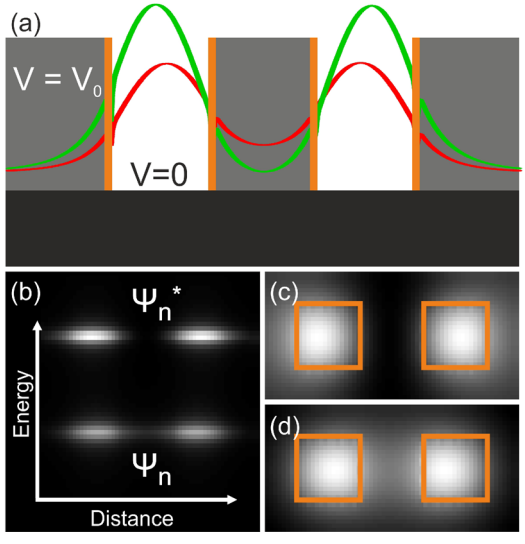

Figure 3. (a) Simplified model of two coupled quantum wells supporting a bonding (red) and antibonding (green) state. (b) Calculated LDOS as a function of electron energy and position along the axis through the centers of the wells (compare with (a)). Ψ_n and Ψ_n^* ($n = 1$) label the bonding and antibonding states, respectively. (c,d) Two-dimensional LDOS maps at the energies of the antibonding (c) and bonding (d) states. The walls of the $\nu = 1$ wells are indicated as orange squares.

dx.doi.org/10.1021/nl403459m | Nano Lett. 2013, 13, 6130−6135

bonding state and an antibonding state are observed. To clearly resolve the bonding and antibonding states in this calculation, we set the imaginary part of the potential, which controls the broadening of the spectral features, to a value of 2 meV. The electron density profiles represented in Figure 3a reveal that the bonding (red) and the antibonding (green) states exhibit different intensities in the central and outer walls. The space-energy map in Figure 3b illustrates this effect. The bonding component is dominant in the region between the QDs, thus leading to an energy feature at that position that is displaced toward lower energy with respect to the isolated QD. In contrast, the antibonding component dominates in the outer walls of the dimer, where it contributes with a feature at higher energy. The 2D maps at the energy of the bonding (Figure 3c) and the antibonding (Figure 3d) states are also showing this effect, which is in good agreement with the experimental observation of Figure 2.

Obviously, the fabrication method introduced in this study is ideally suited to engineer specific arrangements of coupled quantum wells beyond the simple dimer configuration discussed so far. A first example for the interaction of quantum wells in a more sophisticated geometry is presented in Figure 4 and addresses an extended chain of six $\nu = 1$ QDs, which supports a nearly fully developed one-dimensional band structure. Figure 4b shows the resulting broad spectral features in the central cavities of a chain consisting of the six regularly spaced and coupled wells that clearly differ from the electronic structure of rectangular wells of similar length. The distribution of intensity along the energy axis varies significantly from the outer to the central wells. In comparison to an isolated QD (FWHM = 45 meV, green) an additional broadening is observed in Figure 4c not only for the inner wells (FWHM = 91 meV, red) but also for the terminal ones (FWHM = 71 meV, blue). This observation is in excellent agreement with BEM calculation for the same geometry (see Figure 4d,e). Further calculations employing an artificially low imaginary part of the potential, thus resulting in sharp spectral features, illustrate how individual states contribute to the observed intensity distribution in the space-energy map (Figure 4f). Furthermore, a comparison of 6 (see Figure 4f) and 21 coupled trenches (see Figure 4g) that mimic an infinite chain reasonably well,[34] reveals that already for the short chain the full bandwidth of an infinite system is nearly reached. From the experimental data of our six-trench system, we extract an energy spread $\Delta\epsilon$ of ~91 meV, related to the interwell coupling strength. This value is larger but comparable to the bandwidth reported for other periodic molecular structures on metal surfaces supporting dispersive surface state bands.[14]

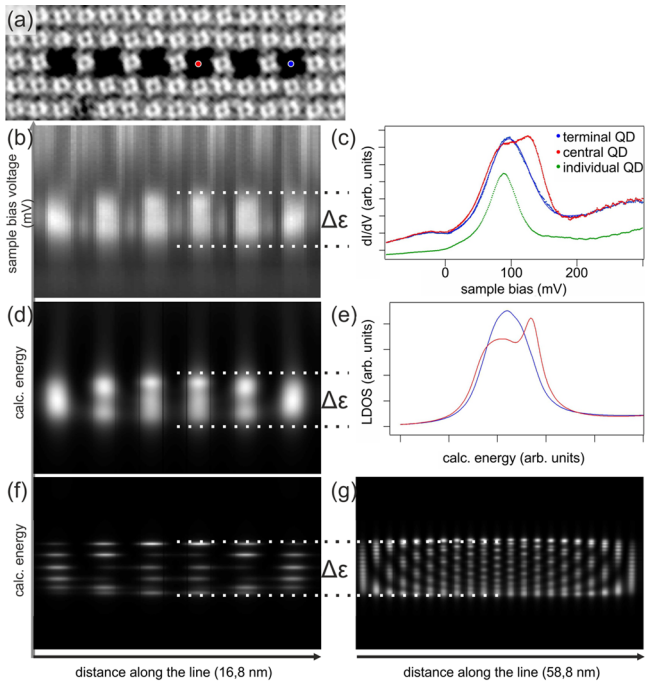

Figure 4. (a) STM image of an artificial chain consisting of six $\nu = 1$ quantum wells in a 2H-TPP array ($U_b = -250$ mV). (b) Spatially resolved STS space-energy map representing 101 single spectra along the axis of the chain presented in (a) (tip positioned at $U_b = -0.1$ V, $I = 0.5$ nA). The spectra in the central cavities are characterized by a broad protrusion exhibiting a width $\Delta\epsilon$ of about 91 meV. (c) Single spectra at the position of an isolated QD (green, FWHM = 45 mV) a terminal QD (blue, FWHM = 71 mV) and a central QD (red, FWHM = 91 mV) of the chain in (a). (d) BEM calculations for the six coupled wells reproducing the LDOS distribution shown in (b). (e) Calculated spectra at the corresponding positions of the chain in good agreement with (c). (f) BEM calculations for the six coupled wells employing an artificially narrow line width in order to clearly resolve the different hybridized states. (g) Analogous simulation for 21 coupled $\nu = 1$ trenches. The full bandwidth $\Delta\epsilon$ is already nearly converged for the six-trench system presented in (b–f).

As a second example, we expand the investigated geometries to a 2D arrangement. To this end, Figure 5 compares a single QD (pseudo 0D) and a linear trimeric structure (1D) with a cross-like assembly (2D) embedded in either Co-TPP or 2H-TPP arrays. For both barrier materials, the spectra recorded in the central cavity are modified when the number of nearest neighbors is increased. Because of the aforementioned leakier walls, the coupling effects are more pronounced for the 2H-TPP system, resulting not only in a broadening but also in a considerable splitting of the spectral feature in the cross-like geometry (Figure 5b). The impact of the interwell interaction is quite subtle for the Co-TPP case, but nevertheless discernible. These experiments prove the tunability of the coupling of artificial quantum wells by a deliberate choice of the barrier material and the geometry that allows us to controllably engineer the electron wave function.

In Figure 5c BEM calculations are shown in excellent agreement with the observed spectra for 2H-TPP, using the aforementioned potential $V = (0.3-0.1i)$ eV. The distance between facing sides of neighboring QDs was set to 0.8 times the side length of a QD square. Considering the simplicity of the model, it is remarkable that theory and experiment agree so closely with a single choice of an effective potential in the molecule region, supplemented by a slight correction in the actual physical separation between the QDs. The evolution of the surface state near the molecules is likely involving complex processes beyond the one-electron picture implicitly assumed in the BEM. The model is however capable of capturing the bold increase in energy and additional splitting of the observed states as more neighbors are added to the structure (see the evolution from the monomer to the dimer in Figure 2c and also to the trimer and pentamer in Figure 5b,c). Notice that this effect could not be directly modeled with a simple description of the interaction between individual QDs in terms of a hopping energy, in the spirit of the tight-binding approach. Actually, this would produce a set of symmetrically positioned states in energy with respect to an unshifted monomer state, and therefore, this model would predict a symmetric splitting

dx.doi.org/10.1021/nl403459m | Nano Lett. 2013, 13, 6130–6135

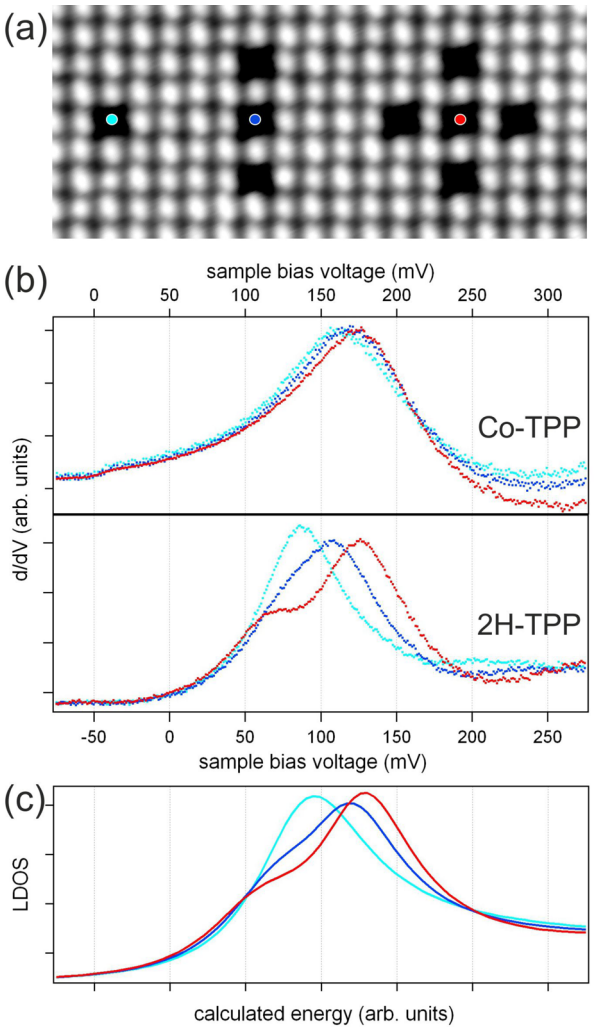

Figure 5. (a) STM image representing quantum wells of a single monomer vacancy, a linear trimer, and a crosslike pentamer in a Co-TPP array (U_b = −666 mV). (b) Modification of the spectral feature induced by adding nearest neighbors in Co-TPP (top) and 2H-TPP (bottom) arrays, respectively. The spectra are taken at the positions of the colored dots in the central cavities (compare (a); tip positioned at U_b = −550 mV, I = 0.3 nA). To highlight the subtle differences in the Co-TPP spectra, they were normalized to the same peak intensity. (c) BEM calculations for the geometries shown in (a) mimicking the 2H-TPP situation. The distance between the quantum wells was set to 0.8 times the QD size.

rather than the observed blue shift. Although an explanation in terms of a complex evolution of different hybridized states would be possible at the cost of adding extra parameters to such tight-binding approach, we consider that the present BEM method presents a sufficient level of physical content (i.e., its relation to the physical geometry of the system and its ability to model the spatial distribution of electron states) and simplicity (only a fitted potential and a correction in gap distance are needed) to intuitively understand the interaction between the neighboring QDs under consideration.

In conclusion, we have introduced a new approach to construct well-defined surface quantum well arrangements and to tune the interwell coupling of unoccupied bound surface states by a suitable choice of the barrier material and the geometry allowing for a controlled wave function engineering. The electronic interaction of two artificial quantum wells of single digit nanometer extension was explored and rationalized with a simple bonding−antibonding model. The potential of this method was demonstrated by the construction of a finite chain and by the assembly of artificial molecules, formed by three or five QDs. The six-QD chain highlights the formation of a one-dimensional electronic band featuring an energy spread yielding a good approximation for the bandwidth of an infinite chain. An increase in the number of next neighbors from zero to four in the artificial molecules considerably modifies the electronic states in the central QD. Finally, the modeling of the experimental data reveals that the coupling of QDs is not in a tight-binding regime, that is, inelastic coupling to the molecular walls and the supporting crystal have to be considered for a complete description of the system. Our approach is of general applicability to molecular arrays on surfaces that support electronic surface states. Our work calls for the exploration of related strategies to further engineer the wave functions of complex coupled systems, as for example using a reduced molecule-surface interaction promoted by a large gap between the highest occupied and lowest unoccupied molecular orbitals, which could lower the absorption of electrons in the molecular barriers and thus yield level splittings exceeding the width of the states involved.

AUTHOR INFORMATION

Corresponding Author

*E-mail: wau@tum.de.

Notes

The authors declare no competing financial interest.

ACKNOWLEDGMENTS

This research project has been supported by the German Research Foundation (DFG) through BA 3395/2-1, the ERC Advanced Grant MolArt (°247299), the DFG Cluster of Excellence Munich Center for Advanced Photonics (MAP), and the Technische Universität München − Institute for Advanced Study (TUM-IAS), funded by the German Excellence Initiative. F.J.G.A. acknowledges support from the Spanish MEC (MAT2010-14885 and Consolider Nano-Light.es).

REFERENCES

(1) Medintz, I. L.; Uyeda, H. T.; Goldman, E. R.; Mattoussi, H. *Nat. Mater.* **2005**, *4*, 435−446.
(2) Bogani, L.; Wernsdorfer, W. *Nat. Mater.* **2008**, *7*, 179−186.
(3) Loss, D.; DiVincenzo, D. P. *Phys. Rev. A* **1998**, *57*, 120.
(4) Ashoori, R. *Nature* **1996**, *379*, 413−419.
(5) Grützmacher, D.; Fromherz, T.; Dais, C.; Stangl, J.; Müller, E.; Ekinci, H. H.; Yasin; Solak; Sigg, H.; Lechner, R. T.; Wintersberger, E.; Birner, S.; Holy, V.; Bauer, G. *Nano Lett.* **2007**, *7*, 3150−3156.
(6) Lan, H.; Ding, Y. *Nano Today* **2012**, *7*, 94−123.
(7) Haider, M. B.; Pitters, J. L.; DiLabio, G. A.; Livadaru, L.; Mutus, J. Y.; Wolkow, R. A. *Phys. Rev. Lett.* **2009**, *102*, 046805.
(8) Crommie, M. F.; Lutz, C. P.; Eigler, D. M. *Science* **1993**, *262*, 218−220.
(9) Heller, E.; Crommie, M. F.; Lutz, C. P.; Eigler, D. M. *Nature* **1994**, *369*, 464−466.
(10) Moon, C.; Mattos, L.; Foster, B.; Zeltzer, G.; Manoharan, H. *Nat. Nanotechnol.* **2009**, *4*, 167−172.
(11) Kliewer, J.; Berndt, R.; Crampin, S. *Phys. Rev. Lett.* **2000**, *85*, 4936−4939.
(12) Crommie, M.; Lutz, C.; Eigler, D.; Heller, E. *Phys. D* **1995**, *83*, 98−108.

(13) Pennec, Y.; Auwärter, W.; Schiffrin, A.; Weber-Bargione, A.; Riemann, A.; Barth, J. V. *Nat. Nanotechnol.* **2006**, *2*, 99−103.
(14) Lobo-Checa, J.; Matena, M.; Müller, K.; Dil, J. H.; Meier, F.; Gade, L. H.; Jung, T. A.; Stöhr, M. *Science* **2009**, *325*, 300−303.
(15) Klappenberger, F.; Kühne, D.; Krenner, W.; Silanes, I.; Arnau, A.; García de Abajo, F.; Klyatskaya, S.; Ruben, M.; Barth, J. V. *Nano Lett.* **2009**, *9*, 3509−3514.
(16) Klappenberger, F.; Kühne, D.; Krenner, W.; Silanes, I.; Arnau, A.; García de Abajo, F. J.; Klyatskaya, S.; Ruben, M.; Barth, J. *Phys. Rev. Lett.* **2011**, *106*, 026802.
(17) Bürgi, L.; Jeandupeux, O.; Hirstein, A.; Brune, H.; Kern, K. *Phys. Rev. Lett.* **1998**, *81*, 5370.
(18) Didiot, C.; Pons, S.; Kierren, B.; Fagot-Revurat, Y.; Malterre, D. *Nat. Nanotechnol.* **2007**, *2*, 617−621.
(19) Sanchez, O.; Garca, J.; Segovia, P.; Alvarez, J.; Vazquez de Parga, A.; Ortega, J.; Prietsch, M.; Miranda, R. *Phys. Rev. B* **1995**, *52*, 7894−7897.
(20) Baumberger, F.; Greber, T.; Delley, B.; Osterwalder, J. *Phys. Rev. Lett.* **2002**, *88*, 237601.
(21) Shiraki, S.; Fujisawa, H.; Nantoh, M.; Kawai, M. *Phys. Rev. Lett.* **2004**, *92*, 096102.
(22) Wallis, T.; Nilius, N.; Ho, W. *Phys. Rev. Lett.* **2002**, *89*, 236802.
(23) Fölsch, S.; Hyldgaard, P.; Koch, R.; Ploog, K. *Phys. Rev. Lett.* **2004**, *92*, 056803−1−4.
(24) Stiufiuc, R.; Perdigão, L.; Grandidier, B.; Deresmes, D.; Allan, G.; Delerue, C.; Stiévenard, D.; Beton, P.; Erwin, S.; Sassi, M. *Phys. Rev. B* **2010**, *81*, 045421.
(25) Cheng, Z.; Luo, M.; Wyrick, J.; Sun, D.; Kim, D.; Zhu, Y.; Lu, W.; Kim, K.; Einstein, T.; Bartels, L. *Nano Lett.* **2010**, *10*, 3700−3703.
(26) Pivetta, M.; Pacchioni, G. E.; Schlickum, U.; Barth, J. V.; Brune, H. *Phys. Rev. Lett.* **2013**, *110*, 086102.
(27) Krenner, W.; Kühne, D.; Klappenberger, F.; Barth, J. V. *Sci. Rep.* **2013**, *3*, 1454.
(28) Comanici, K.; Buchner, F.; Flechtner, K.; Lukasczyk, T.; Gottfried, J. M.; Steinrück, H.-P.; Marbach, H. *Langmuir* **2008**, *24*, 1897−1901.
(29) Auwärter, W.; Seufert, K.; Klappenberger, F.; Reichert, J.; Weber-Bargioni, A.; Verdini, A.; Cvetko, D.; Dell'Angela, M.; Floreano, L.; Cossaro, A.; Bavdek, G.; Morgante, A.; Seitsonen, A. P.; Barth, J. V. *Phys. Rev. B* **2010**, *81*, 245403.
(30) Li, J.; Schneider, W.-D.; Berndt, R.; Crampin, S. *Phys. Rev. Lett.* **1998**, *80*, 3332−3335.
(31) Morgenstern, K.; Braun, K. F.; Rieder, K. H. *Phys. Rev. Lett.* **2002**, *89*, 226801.
(32) Gross, L.; Moresco, F.; Savio, L.; Gourdon, A.; Joachim, C.; Rieder, K.-H. *Phys. Rev. Lett.* **2004**, *93*, 056103.
(33) Hieringer, W.; Flechtner, K.; Kretschmann, A.; Seufert, K.; Auwärter, W.; Barth, J. V.; Görling, A.; Steinrück, H.-P.; Gottfried, J. M. *J. Am. Chem. Soc.* **2011**, *133*, 6206−6222.
(34) Nilius, N.; Wallis, T.; Ho, W. *Science* **2002**, *297*, 1853−1856.
(35) Ashcroft, N.; Mermin, D. *Solid State Physics*; Saunders College Publishing: New York, 1976.
(36) Crain, J.; Pierce, D. *Science* **2005**, *307*, 703−706.

dx.doi.org/10.1021/nl403459m | *Nano Lett.* 2013, 13, 6130−6135